

Making a splash with water repellency

CYRIL DUEZ¹, CHRISTOPHE YBERT¹, CHRISTOPHE CLANET² AND LYDÉRIC BOCQUET^{1*}

¹Laboratoire PMCN, Université Lyon 1, UMR CNRS 5586, 69622 Villeurbanne, France

²IRPHE, UMR CNRS 6594, 13384 Marseille, France

*e-mail: lyderic.bocquet@univ-lyon1.fr

Published online: 25 February 2007; doi:10.1038/nphys545

A splash is usually heard when a solid body enters water at large velocity. This phenomenon originates from the formation of an air cavity during the impact. The classical view of impacts on free surfaces relies solely on fluid inertia; therefore, surface properties and viscous effects should be negligible at sufficiently large velocities. In strong contrast to this large-scale hydrodynamic viewpoint, we demonstrate here that the wettability of the impacting body is a key factor in determining the degree of splashing. This unforeseen fact is further embodied in the dependence of the threshold velocity for air entrainment on the contact angle of the impacting body, as well as on the ratio between surface tension and fluid viscosity, thereby defining a critical capillary velocity. As a paradigm, superhydrophobic impactors make a big splash for any impact velocity.

The first systematic study of splashes was published more than one century ago by Worthington¹. In this pioneering work, he used high-speed photography to examine impacts of drops and solid bodies on a liquid surface, with beautiful illustrations of splashes. (For impact of solid spheres on a liquid, it is interesting to mention that Worthington did observe different splashing behaviours, referred to as ‘rough’ or ‘smooth’, which are similar to the wettability effect discussed in the present paper.) In recent years, there has been a resurgence of interest in the physics of impact, due in particular to the development of rapid video imaging. And new perspectives have emerged, showing that unforeseen mechanisms play a central role in impact: to cite a few, the inhibition of droplet rebound by adding tiny amounts of polymers², the complex deformation dynamics of a rebounding drop³ and the unexpected role of ambient air on drop splashing^{4,5}. Here, we consider the situation of a solid body impacting a gas–liquid interface. This situation is obviously relevant for many naval applications, such as ship slamming and air to sea weapons, and for any industrial coating process that involves the dipping of a solid object in a liquid bath (where air entrainment is to be avoided). The traditional description of an impact of a solid body on a free interface follows the work of von Karman and Wagner^{6,7}, in which viscosity, surface tension and compressibility effects are neglected^{8,9}. This idealized framework is formally justified by the fact that in the situations relevant to impacts, the Reynolds Re and Weber We numbers, quantifying the role of inertia versus respectively viscous and capillary effects, are very large. This is precisely the regime of interest in this study: $Re = \rho U a / \mu_L \gtrsim 10^4 - 10^5$ and $We = \rho U^2 a / \gamma_{LV} \gtrsim 10^3 - 10^4$ (for impacting body diameter a , velocity U , liquid density ρ , liquid viscosity μ_L and liquid–vapour surface tension γ_{LV}). Accordingly, capillarity and viscosity are not expected to play any role in the impact and can be ignored in this description.

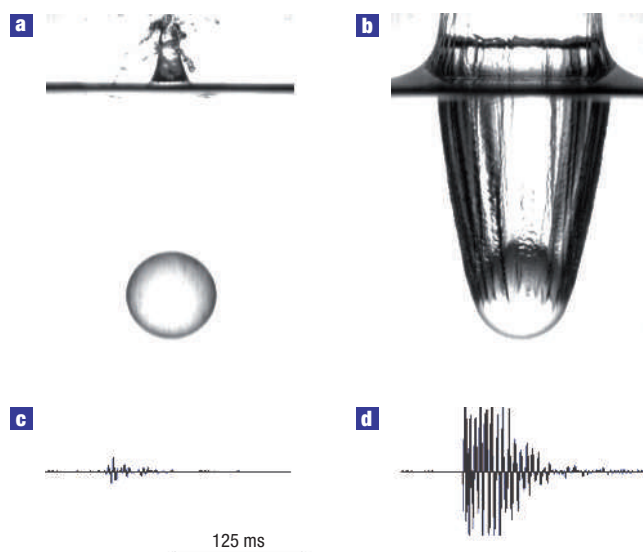


Figure 1 Visual and audio recordings of impact. **a,b**, Photographs of the impact of two spheres differing only in wettability by a nanometric coating on their surface: impact of a perfectly wetting sphere, with static contact angle $\theta_0 \simeq 15^\circ$ (**a**); impact of a hydrophobic sphere with static contact angle $\theta_0 \simeq 100^\circ$ (**b**). The impact velocity was 5.0 m s^{-1} in both cases, corresponding to a 1.25 m height drop. The photographs were taken 15.5 ms (**a**) and 15.0 ms (**b**) after initial impact. **c,d**, Time-dependent audio recordings of the impacts, as measured by a microphone $\sim 10 \text{ cm}$ from the impact point, for a hydrophilic (**c**) and a hydrophobic (**d**) sphere. The signal is proportional to the acoustic pressure emitted during the impact. The units on the vertical scale are arbitrary (but identical). A big ‘splash’ is evident for the hydrophobic sphere, whereas a tiny ‘plop’ is heard for the hydrophilic sphere. The sound is associated with the rapid closure of the cavity (not shown).

Our experimental results contrast with this simple picture. As illustrated in Fig. 1, two spheres that differ only by a nanometric coating that modifies wettability exhibit very different impact behaviour: a huge air cavity is entrained for the hydrophobic sphere, whereas no such behaviour is observed for the hydrophilic sphere. However, apart from the static contact angle ($\theta_0 \simeq 15^\circ$ versus $\theta_0 \simeq 100^\circ$), the spheres are identical in terms of bulk material (glass), diameter, very low surface roughness and impact velocity ($U = 5 \text{ m s}^{-1}$). Moreover, during the experiment, a ‘splash’ is heard for the hydrophobic sphere, whereas only a tiny ‘plop’ is produced by the hydrophilic sphere, as shown in Fig. 1c,d.

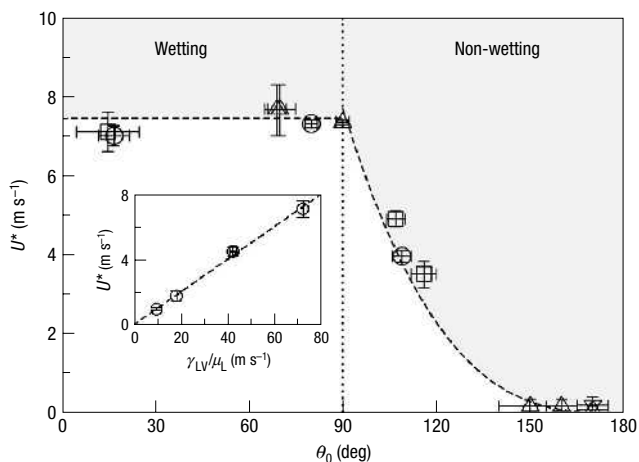


Figure 2 Threshold velocity U^* for air entrainment as a function of (advancing) static contact angle θ_0 of the impacting body. The dashed lines are the theoretical predictions based on relations (1) and (2). The shaded area is the splash domain. The different symbols correspond to different bead diameters—square: 25.4 mm (glass); down-triangle: 20 mm (aluminium); circle: 15 mm (glass, steel); up-triangle: 7 mm (aluminium, steel). The beads are covered with various coatings to modify their wettability (see the Methods section). To focus on wettability as the only surface parameter, only smooth objects have been considered in the present study (see the Methods section). Inset: Dependence of the threshold velocity for a wetting glass sphere (25.4 mm) on the ratio γ_{LV}/μ_L . We used various liquids to explore this dependence: water, isopropanol, ethanol and a water–glycerol mixture (20 wt% of glycerol). For these fluids, the contact angle on the sphere surface was always below 10° . The dashed line is a linear prediction $U^* = \xi \gamma_{LV}/\mu_L$ (with $\xi \approx 0.1$).

This observation raises puzzling questions: how can a nanometric coating modify large-scale hydrodynamics? More generally, how might capillarity affect the flow pattern in the limit of large Weber numbers? To answer these questions, we have first explored the conditions required to create an air cavity, as illustrated in the above example. By varying the velocity of the impacting body, we have demonstrated that an air cavity is created during an impact only above a threshold velocity, U^* , typically of a few metres per second. Furthermore, this threshold velocity is found to depend on the (advancing) contact angle θ_0 of the impacting body. The experimental results for U^* in water are shown in Fig. 2 for spheres with various wettabilities. Going further, we measured the dependence of the threshold velocity U^* on the liquid properties, by considering impacts on various liquids (with different viscosities and surface tensions) for fixed wettability. As shown in the inset of Fig. 2, we found that U^* is proportional to the capillary velocity, defined as γ_{LV}/μ_L . To complete this exploration, we verified that the diameter of the impacting sphere does not influence the threshold (see Fig. 2), nor does the gas pressure (varied between 0.1 and 1 atm).

To rationalize these results, we focus on the detailed dynamics of the impact. An essential characteristic of solid to liquid impacts is that a thin film develops during the impact and climbs up the impacting body¹⁰. This film is evident in Fig. 3a. However, the film dynamics is seen to strongly differ depending on whether the velocity is below or above the threshold U^* for air entrainment. For the velocity considered in Fig. 3, the hydrophilic sphere is below the threshold: the film is seen to follow the sphere and closes up at the pole of the sphere (Fig. 3a). As such, no cavity is created. On the contrary, for the same velocity, the hydrophobic sphere is above threshold and the film is seen to detach from the sphere before

reaching the pole (Fig. 3b). The opened aperture left at the top of the sphere then leads to cavity formation and air entrainment. These pictures thus point to the film dynamics as the origin of air entrainment and splash.

We therefore propose an interpretation of these results in terms of contact-line stability. The geometry is described in Fig. 3c. The liquid film and triple line move at a velocity v of $v \approx \zeta U$, with ζ a numerical prefactor of order unity (see ref. 8). Let us first consider the motion of the film on a hydrophobic sphere. In this case, the gas (air) is the wetting phase and the solid surface moves towards the non-wetting phase (liquid). This situation corresponds to the prototypical problem of forced (de)wetting, but here with the air replacing the liquid in the role of the wetting phase, see Fig. 3c. Since the work of de Gennes¹¹, it has been known that a critical speed exists above which the triple line is no longer stable, as the dynamic contact angle θ_d goes to 180° (ref. 12). Above this critical speed, the solid will be coated by the wetting phase, here air. A hydrodynamic force balance at the contact line shows that this occurs at a critical capillary number $Ca^* = \mu v^*/\gamma_{LV}$ obeying $Ca^* \approx \theta_0^3/9\ell$, with θ_0 being the static contact angle as defined with respect to the wetting phase (air) and $\ell \approx 15$ – 20 , see refs 11,12. Using $\theta_0 = \pi - \theta_d$, we get $Ca^* \approx (\pi - \theta_d)^3/9\ell$. This classical reasoning, however, neglects dissipation in the non-wetting phase (here water). This assumption is obviously not valid. We have added a liquid viscous contribution in the force balance at the triple line, in the form $F_L \approx C\mu_L v$ (with $C \sim 1$). This term adds to the classical contribution in the wetting phase corner, here $F_{\text{air}}(v) = (3\mu_{\text{air}}\ell/[\pi - \theta_d])v$, diverging as $\theta_d \rightarrow 180^\circ$. Both terms are of the same order of magnitude as $\alpha = 3\ell\mu_{\text{air}}/\mu_L \sim 1$. Using this new expression for the frictional force, the critical velocity is found to be of the form $v^* = (g_0/9\ell)(\gamma_{LV}/\mu_L)[\pi - \theta_0]^3$, defining a critical capillary number in terms of the liquid viscosity. The numerical prefactor g_0 is typically of the order of ~ 5 – 10 , with a weak dependence on the liquid and gas viscosity. Using $v = \zeta U$, we eventually get the threshold velocity for non-wetting impactors ($\theta_0 \geq 90^\circ$),

$$U^* = \frac{g_0}{9\ell\zeta} \frac{\gamma_{LV}}{\mu_L} [\pi - \theta_0]^3. \quad (1)$$

As shown in Fig. 2, this theoretical prediction is in very good agreement with the experimental results with hydrophobic impactors ($\theta \geq 90^\circ$). This mechanism culminates in the superhydrophobic limit, for which the impacting body entrains air for any velocity. Fixing $\ell = 15$ and $\zeta = 2$, experimental results are quantitatively reproduced with $g_0 \approx 7$ (which corresponds to $C \approx 2.9$).

The situation of a hydrophilic impacting sphere may be discussed along the same lines. Although the contact angle is lower than 90° for small velocities, the dynamical contact angle θ_d will increase with the triple-line velocity v . As above, the triple line will disappear as $\theta_d \rightarrow 180^\circ$ (ref. 12). Unfortunately, no analytical description is available for $\theta_d(v)$ in this limit when starting from a wetting surface ($\theta_0 \leq 90^\circ$). Nevertheless, the physics is qualitatively similar to that described above for the non-wetting surfaces and the dissipation in air, which diverges as $\theta_d \rightarrow 180^\circ$, will destabilize the contact line above a threshold velocity. We therefore expect again a critical velocity, scaling as in the previous case like

$$U^* \approx \xi \frac{\gamma_{LV}}{\mu_L}. \quad (2)$$

The prefactor ξ may depend on the static contact angle θ_0 . However, as at the threshold for destabilization $\theta_d^* \sim \pi$ is significantly larger than the static contact angle θ_0 , we only expect a weak dependence of ξ on θ_0 . This point is confirmed experimentally, as shown in Fig. 2: in the wetting regime the critical velocity for

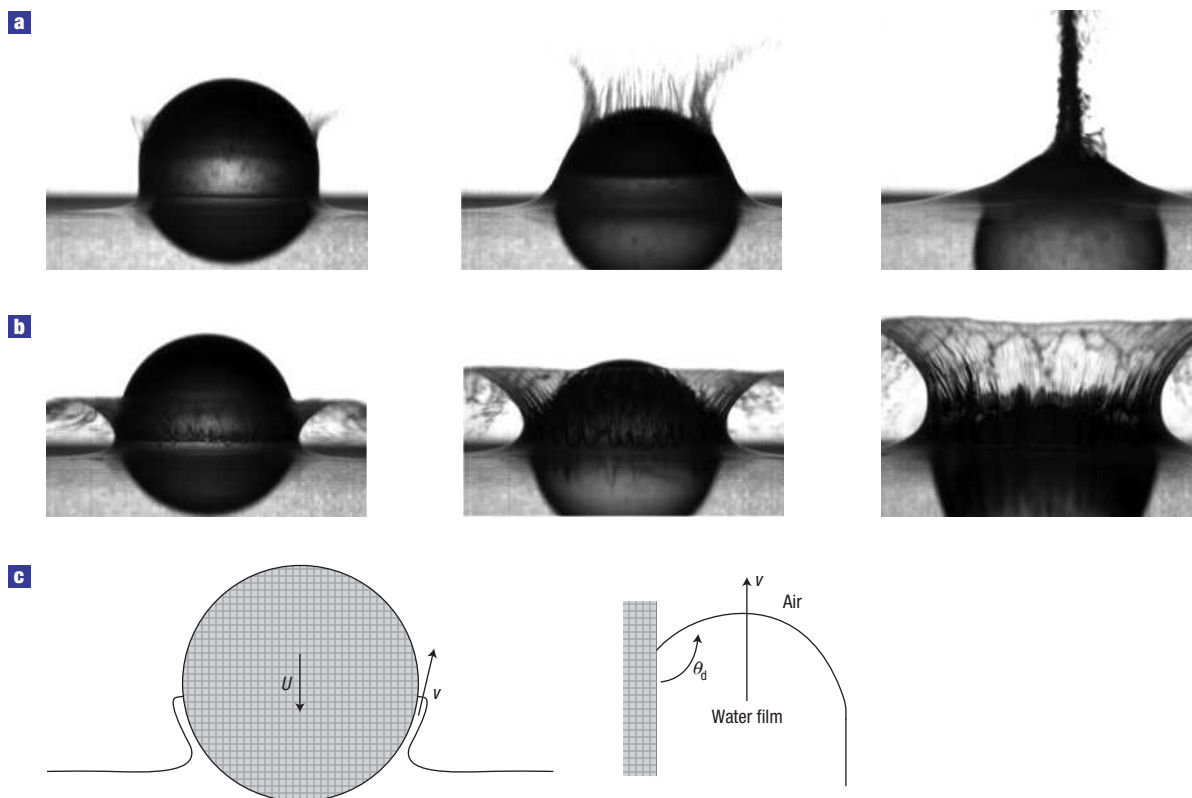


Figure 3 Detailed chronophotography of impacting spheres with two different wettabilities at the same impact velocity $U = 5 \text{ m s}^{-1}$. **a**, Hydrophilic sphere (1.4, 2.2 and 3.9 ms after initial impact). **b**, Hydrophobic sphere (1.5, 2.4 and 4.0 ms after initial impact). For the hydrophilic sphere, the considered impact velocity is below the threshold for air entrainment: the ascending film is shown to follow the sphere and gather at the pole. For the hydrophobic sphere, the impact velocity is above the threshold for air entrainment: the ascending film detaches from the sphere, thereby creating a cavity during the impact. **c**, Left: Diagram of the impact geometry; right: magnification of the triple-line region. θ_d is the dynamic contact angle, which is larger than the static contact angle θ_0 for a moving triple line (with velocity v). The threshold velocity is reached as the contact line is no longer stable, which occurs as $\theta_d \rightarrow 180^\circ$.

air entrainment is basically independent of the static contact angle. Moreover, changing the fluid fully confirms the linear dependence of U^* on γ_{LV}/μ_L as embodied in expression (2) (see Fig. 2, inset). Comparison with experimental results suggests $\xi \approx 0.1$ (see Fig. 2, inset).

We finish with a short discussion on the ‘splashing’ sound, which can be heard above threshold (see Fig. 1). The sound arises from the rapid closure of the cavity as it pinches off. These dynamics are gravity driven so that the closure time is typically $\tau \sim \sqrt{a/g}$, where a is the size of the impacting object and g is the gravitational constant^{13,14}. For a centimetre body, $\tau \sim 100 \text{ ms}$, in full agreement with the recordings shown in Fig. 1 (to compare with the impact time $a/U \sim 5 \text{ ms}$ in this case). As we confirmed independently, the splash duration and amplitude are therefore independent of the impact velocity.

METHODS

SURFACE TREATMENTS TO CONTROL WETTABILITY

We use spheres made of glass, steel and aluminium, with diameters varying between 7 and 25.4 mm.

Wetting glass beads ($\theta_0 \approx 15\text{--}20^\circ$) are obtained by immersion for 40 min in piranha solution (1 vol H_2O_2 , 2 vol H_2SO_4), then rinsed using deionized water and isopropanol, and finally heated at 110°C for 20 min.

Hydrophobic glass beads ($\theta_0 \approx 100\text{--}120^\circ$) are obtained by grafting silane chains on the surface. We chose grafting of octyltriethoxysilane (105°) or

perfluorooctyltrichlorosilane ($110\text{--}120^\circ$) in the gas phase (by pumping in a closed vessel), for 15 h at ambient temperature. After silanization, the beads are rinsed with isopropanol, dried and heated at 90°C for 1 h.

Superhydrophobic aluminium beads ($\theta_0 \approx 150\text{--}170^\circ$) are obtained following the chemical protocol proposed by Qian and Zhen¹⁵. The aluminium beads are first plunged into an aqueous solution of chlorhydric and fluorhydric acids for 15 s. Then a silane coating (perfluorooctyltriethoxysilane) is grafted on the beads by silanization in the liquid phase at ambient temperature for 1 h and then heated at 130°C for 1 h. This protocol works only for pure aluminium and we therefore used 1,050 Al.

The contact angle on the steel beads is $\theta_0 \approx 80\text{--}90^\circ$, obtained after cleaning with deionized water with detergent, and then with isopropanol. An atomic force microscope (AFM) topographic scan of the beads’ surface shows that for the beads considered in this study, the peak-to-peak roughness was smaller than 100 nm (with a r.m.s. roughness of $\sim 5 \text{ nm}$ for a $10 \mu\text{m} \times 10 \mu\text{m}$ scan). Larger scale roughness was probed with a profilometer (Tencor Instruments) with a $5 \mu\text{m}$ tip showing less than 20 nm r.m.s. deviation over a millimetre scan. For the superhydrophobic coatings, we have shown moreover in a previous work using AFM measurements that the liquid interface on the coatings is very smooth with a peak-to-peak roughness in the hundreds of nanometres range¹⁶.

IMPACT EXPERIMENT SET-UP AND PROTOCOL

The beads are released from rest at varying heights above a transparent box containing the liquid. The impact is recorded using a high-speed video camera (Mikrotron) at a frame rate of $\sim 1,000$ frames per second. The impact speed is determined from the movie. Before each release, the beads are cleaned by rinsing with isopropanol, dried using nitrogen and heated at 110°C for 20 min for a complete drying. We left the beads to cool to ambient temperature before

impact. Most of our experiments are conducted with water, but to study the effect of fluid properties (viscosity, surface tension) we use ethanol, isopropanol and a water–glycerol mixture (20 wt% of glycerol) to vary the viscosity. The contact angle on the bare glass beads with these fluids was always smaller than 10° . The viscosity of the water–glycerol mixture was measured before and after each impact using a Ubbelohde viscometer. The values for the surface tensions were taken from the literature.

Received 16 November 2006; accepted 22 January 2007; published 25 February 2007.

References

1. Worthington, A. M. & Cole, R. S. Impact with a liquid surface studied by the aid of instantaneous photography II. *Phil. Trans. R. Soc. Lond. A* **194**, 175–199 (1900).
2. Bergeron, V., Bonn, D., Martin, J.-Y. & Vovelle, L. Controlling droplet deposition with polymer additives. *Nature* **405**, 772–775 (2000).
3. Richard, D., Clanet, C. & Quéré, D. Contact time of a bouncing drop. *Nature* **417**, 811 (2002).
4. Xu, L., Zhang, W. W. & Nagel, S. R. Drop splashing on a dry smooth surface. *Phys. Rev. Lett.* **94**, 184505 (2005).
5. Quéré, D. Impact on Everest. *Nature* **435**, 1168 (2005).
6. von Kármán, T. The impact on seaplane floats during landing. NACA Technical Note 321 (1929).
7. Wagner, H. Phenomena associated with impacts and sliding on liquid surfaces. *Z. Angew. Math. Mech.* **12**, 193–215 (1932).
8. Oliver, J. *Water Entry and Related Problems*. Thesis, Oxford Univ. (2002).
9. Howison, S., Ockendon, J. R. & Oliver, J. M. Oblique slamming, planing and skimming. *J. Eng. Math.* **48**, 321–337 (2004).
10. Korobkin, A. A. & Pukhnachov, V. V. Initial stages of water impact. *Annu. Rev. Fluid Mech.* **20**, 159–185 (1988).
11. de Gennes, P.-G., Brochard-Wyart, F. & Quéré, D. *Gouttes, bulles, perles et ondes* (Belin, Paris, 2005).
12. Eggers, J. Hydrodynamic theory of forced dewetting. *Phys. Rev. Lett.* **93**, 094502 (2004).
13. Glasheen, J. W. & McMahon, T. A. Vertical water entry of disks at low Froude numbers. *Phys. Fluids* **8**, 2078–2083 (1996).
14. Duclaux, V. *et al.* Dynamics of transient cavities. *J. Fluid Mech.* (2007) (in the press).
15. Qian, B. & Shen, Z. Fabrication of superhydrophobic surfaces by dislocation-selective etching on aluminium, copper and zinc substrates. *Langmuir* **21**, 9007–9009 (2005).
16. Journet, C., Moulinet, S., Ybert, C., Purcell, S. T. & Bocquet, L. Contact angle measurements on superhydrophobic carbon nanotube forests: Effect of fluid pressure. *Europhys. Lett.* **71**, 104–109 (2005).

Acknowledgements

This project was supported by the French Ministry of Defense, via DGA. L.B. would like to thank J.-F. Pinton for discussions on the subject and D. Huang for a careful reading of the manuscript. The authors thank S. Manneville for kindly lending us the high-speed video system and M.-C. Audry for the AFM scans.

Correspondence and requests for materials should be addressed to L.B.

Competing financial interests

The authors declare that they have no competing financial interests.

Reprints and permission information is available online at <http://npg.nature.com/reprintsandpermissions/>